

Chapter 4

Photocurrent Generation in
Reduced Graphene

Oxide-Cadmium Zinc Sulfide
(*RGO – Cd_{0.5}Zn_{0.5}S*)

Nanocomposite and its
Photocatalytic Performance
towards *PNP* Degradation.

4.1 Introduction

The extraordinary electronic and optoelectronic properties of reduced graphene oxide (*RGO*) make it a potential candidate in the present age [223-226]. The surface defects, wide range of oxygen functionalities at the edges and irregular structure of *RGO* sheet serves as an ideal canvas for anchoring metal, metal oxide, polymer, semiconductor nano materials [227-231]. *RGO* based multifunctional materials can be easily synthesized, where no binder or any connector is required. Recently, different photosensitive semiconductor nano materials have been attached on the epoxy position of carbons of two layers of *RGO* by using different techniques [222, 195]. In these nano composite systems *RGO* offers continuous pathway for electron transfer. At the same time *RGO* hinder the recombination probability of the photo generated electron – holes present in photoactive material, preventing the self aggregation of nano materials. Tremendous efforts have been focused towards the development of *RGO* based nano composites for their application as solar cells, photo diodes, photo transistor materials [217, 221, 229]. So far, different semiconducting nanomaterials, such as *TiO₂*, *ZnO*, *CdS*, *ZnS*, *PbS* etc has been anchored with *RGO*, for different optoelectronic applications through photo induced charge generation under the illumination of radiation varying from ultraviolet to infrared [232-235]. To this end ternary chalcogenide nano materials have fascinated remarkable interest as a prospective candidate for next generation optoelectronic applications because of their easy tunability of optical band gap by simply changing the weight ratio of their counterparts [236, 237]. For an example, cadmium zinc sulfide (*Cd_{1-x}Zn_xS*) tertiary alloy

has the potential to form a continuous series of solid solutions and allows to reveal the prospect to vary the optical band gap from visible ($CdS = 2.42 eV$) to ultraviolet ($ZnS = 3.7 eV$) region. The composition and shape controlled optical properties of $Cd_{1-x}Zn_xS$ composite was studied extensively [237].

On the other hand, great attention has been devoted to use photocatalytic degradation of organic water pollutant through the photo induced charge generation [235, 238]. Among various aromatic compounds, phenol and phenolic compounds are common contaminants in industrial and agricultural wastewater due to their high toxicity and persistence in water [239-241]. Although, there are few reports on the photocurrent generation and photocatalytic hydrogen production using $RGO - CdZnS$ composite [239], but neither of these studies explores the photocatalytic degradation of 4-nitrophenol (4- NP). Li et.al reported a thermolysis method for the preparation of $Cd_{1-x}Zn_xS$ solid solution with enhanced visible light photocatalytic H_2 production [242]. In recent year, researchers fabricated $RGO - CdZnS$ composite as a potential photocatalyst with enhanced solar light responsive photocatalytic hydrogen production and dye degradation [238, 243]. The close contact between RGO and $CdZnS$ facilitate the prompt transfer of the photoinduced electrons from the conduction band of $CdZnS$ to RGO , which significantly increases the stability of the photocatalyst by preventing the reduction of Zn^{2+} and Cd^{2+} [238, 243].

Here, we report the photocurrent generation of simple low cost one pot single step solvothermally synthesized RGO decorated $Cd_{1-x}Zn_xS$ nano rod alloy composite under simulated solar light illumination. We have chosen the value of x as 0.5 for the adjustment of the material working in the mid-

dle range between *UV* and *Vis.* of solar spectra. The micro morphological structure was confirmed by *X-ray* Diffraction (*XRD*), Transmission Electron Microscopy (*TEM*) analysis. The formation of *CdZnS* and reduction of *GO* were confirmed by Raman spectroscopy. The optical properties were characterized by *UV – Vis* spectroscopy. The photo induced charge transformation from *CdZnS* nanorods to *RGO* sheet through the interface of *RGO – CdZnS* nano composite were confirmed by steady state photoluminescence (*PL*) spectroscopy. The optoelectronic properties of *RGO–CdZnS*, under simulated solar light irradiation, were investigated by fabricating large area thin film photodetector using *RGO – CdZnS* as an active material. As-prepared composite exhibited excellent photo response properties. We have also studied the variation of photosensitivity with the intensity of incident light. Furthermore, the possible mechanism for photocurrent generation of *RGO – CdZnS* system is also anticipated.

4.2 Experimental Section

4.2.1 Materials Used

Graphite powder, potassium persulfate [$K_2S_2O_8$], phosphorus pentoxide [P_2O_5], zinc acetate dihydrate [$Zn(CH_3COO)_2, 2H_2O$], cadmium acetate dihydrate [$Cd(CH_3COO)_2, 2H_2O$], thiourea [NH_2CSNH_2] and sodium nitrate [$NaNO_3$] were purchased from Sigma Aldrich; Ethylenediamine [$EN, NH_2CH_2CH_2NH_2$], Potassium permanganate [$KMnO_4$], hydrogen peroxide [H_2O_2], hydrochloric acid [HCl], sulfuric acid [H_2SO_4] were purchased from Merck, India. All

the materials were of analytical grade and used as received without further purification.

4.2.2 Materials Preparation

4.2.2.1 Synthesis of Graphene Oxide (GO)

GO was synthesized by the oxidation of natural graphite powder via modified Hummers' method [244] as stated in introduction chapter.

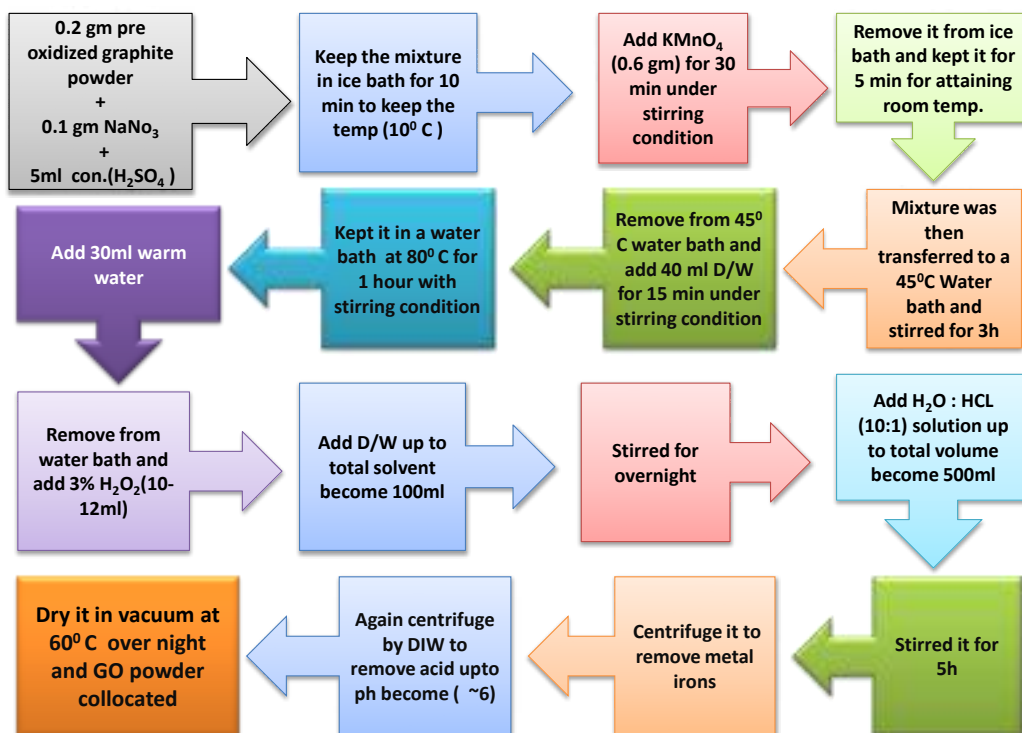


Figure 4.2.1: GO Synthesis diagram

4.2.2.2 Synthesis of RGO-CdZnS Nanocomposites and Controlled CdZnS

For one pot single step synthesis of *RGO – CdZnS*, 0.11 g (0.5 mM) of zinc acetate dehydrate, 0.133 g (0.5 mM) of cadmium acetate dihydrate and 0.228 g (3 mM) of thiourea were taken in a Teflon lined stainless steel autoclave. 80 % of the total volume of the autoclave was filled up with the *EN* and double distilled water *DDW* (2 : 1) mixture. The resultant mixture was stirred and 60 mg *GO* was poured to the solution, followed by ultra sonication for 15 min.

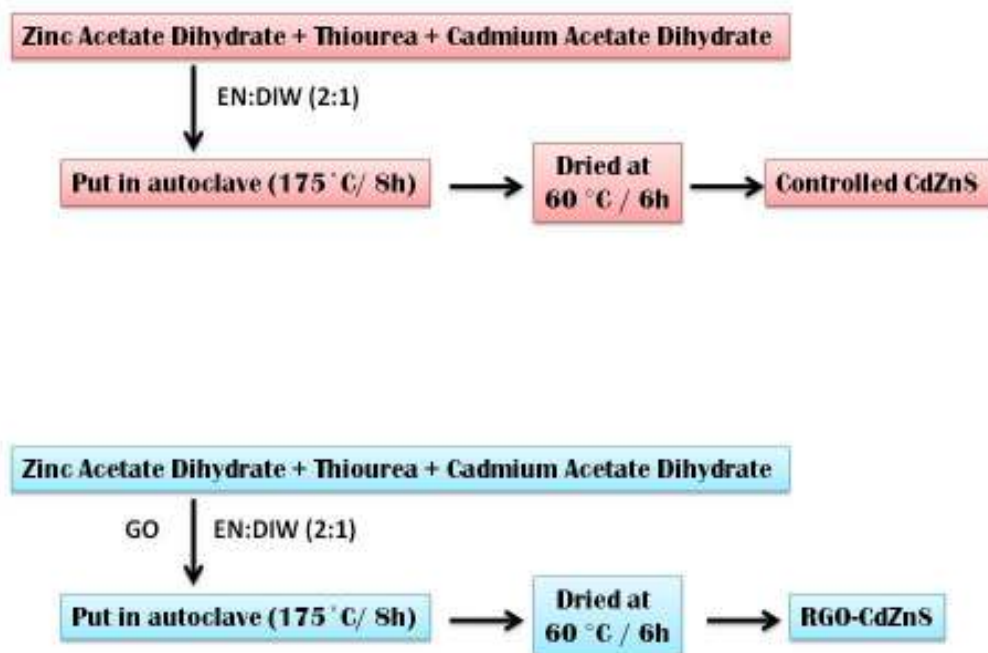


Figure 4.2.2: Synthesis of *CdZnS* nano rod and *RGO – CdZnS* nano composite

Then the solution was transferred to autoclave and kept inside a preheated oven at 175°C for 8 hour. After achieving room temperature, the resulting precipitates were separated by centrifugation for three times at 8000 rpm and washed by *DDW* and ethanol. Then the *RGO – CdZnS* sample was dried at 60°C for 6 h. The controlled *CdZnS* nanorod was synthesized followed by same method in absence of *GO*.

4.3 Material characterization

The samples were characterized by *XRD* (Rigaku-Miniflex *II*) with *Cu-K α* radiation ($= 0.15418\text{ nm}$) operated at 30 kV and 10 mA . *TEM* images were collected on *JEOL* 2010 operated at 200 kV and using copper grid. Raman spectra were recorded from powder samples of controlled *CdZnS*, *GO* and *RGO–CdZnS* at room temperature using an Invia Raman microscope equipped with a 514 nm excitation laser. *UV – Vis* spectra were collected from a Shimadzu *UV – 1700 UV-Vis.* spectrometer. *PL* spectra were collected from Perkin Elmer *LS 55* spectrofluorometer at ambient temperature.

4.4 Device Fabrication and Opto-electrical Transport Measurement

We have fabricated a thin film photo detector to investigate the photo induced current generation under simulated solar light irradiation. The thin film was prepared by simply drop casting from a dispersed solution of *RGO–CdZnS* in iso-propyl alcohol (*IPA*) on a pre-cleaned glass substrate. After

drop casting, the sample was kept to dry for few hours. A pair of parallel electrodes was drawn using conducting silver paint (Ted Pella). A Keithley 2611A source meter was used to study the voltage (V) – current (I) characteristics under darkness and solar light illumination (Newport, Oriel 67005, AM 1.5) with different intensity. The data was collected by Lab –Tracer 2.0 interfaced with the data acquisition card. The optical power was measured by an optical power meter (Newport 843–R).

4.5 Result and discussion

The *XRD* was employed to confirm the structural composition of materials (pristine Graphite, *GO*, *RGO*, controlled-*CdZnS* and *RGO – CdZnS* composite) and the diffraction patterns are presented in Figure 4.5.1A. In pristine Graphite the peak centered at $2\theta = 26.3^\circ$ depicts inter planer spacing of 0.337 nm . This peak shifts to $2\theta = 10.5^\circ$, with d -spacing of 0.87 nm confirms the oxidation of graphite and formation of *GO* [245]. After reduction of *GO* the sharp peak totally vanishes and a hump at $2\theta = 24.5^\circ$ with d -spacing of 0.34 nm , is observed in the *XRD* pattern of *RGO*. The controlled-*CdZnS* and *RGO – CdZnS* composite illustrate similar diffraction pattern with peaks indexed as (100), (002), (101), (102), (110), (103) and (200) [242]. Position of all the peaks of *CdZnS* remain unaltered in *RGO – CdZnS* gives the major support of formation of crystalline alloy semiconductor in *RGO – CdZnS* nano composite. Absence of peak shift ruled out the possibility of any significant change in crystalline phase of *CdZnS* after formation of composite. Diffraction peak for *RGO* is not clearly observable in *RGO – CdZnS* proba-

bly due to very low diffraction intensity of graphitic planes compare to high crystallinity of $CdZnS$.

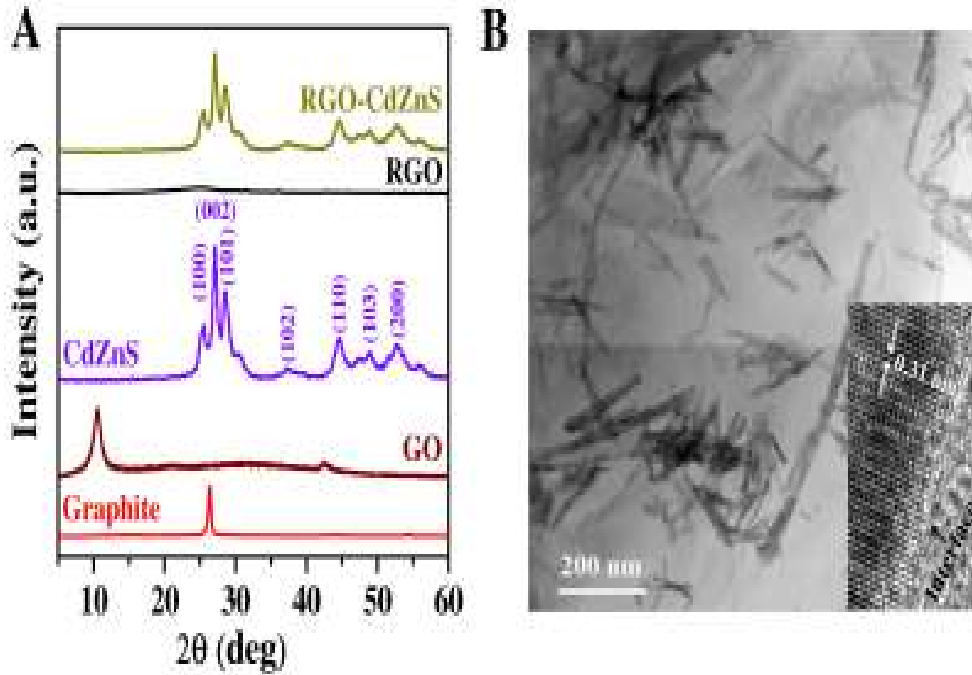


Figure 4.5.1: (A) The XRD patterns of Graphite, GO , controlled $CdZnS$, RGO and $RGO - CdZnS$ composite. (B) TEM image of $RGO - CdZnS$ composite. The $HRTEM$ image of $RGO - CdZnS$ is shown in the inset of (B).

The morphology and nano structure formation in $RGO - CdZnS$ composite was studied by TEM image analysis and is presented in Figure 4.5.1B. It is clearly observed that $CdZnS$ nanorods of length nearly 100 nm and width $10 - 12\text{ nm}$ are well anchored on the two dimensional RGO sheet. To check the crystallinity of the $CdZnS$ on the RGO sheets and to examine the possibility of formation of $CdZnS - RGO$ core-shell structure, we have also studied the $HRTEM$ image. The $HRTEM$ image (inset of Figure 4.5.1B) reveals the well crystallinity of $CdZnS$ and the measured lattice fringe spacing is

about 0.31 nm , can be assigned to the (101) lattice plane of the hexagonal $CdZnS$. The *HRTM* image also confirms that there is no signature of core shell structure formation in the composite materials.

Figure 4.5.2A and 4.5.2B show the micro-Raman spectra of controlled- $CdZnS$, *GO* and *RGO* – $CdZnS$ composite. Figure 4.5.2A shows peaks correspond to the scattering from 1 *LO* and 2 *LO* phonon modes [246, 247] of $CdZnS$. The reduction of *GO* was confirmed by the changes in relative intensity of *D* and *G* band peaks. Figure 4.5.2B shows the micro-Raman spectra of the *GO* and *RGO* – $CdZnS$ composite. The *D* band located at 1350 cm^{-1} in the Raman spectra depicts the lattice distortions. Whereas, the *G* band located at 1585 cm^{-1} corresponding to the first-order scattering of the E_g^2 mode [248].

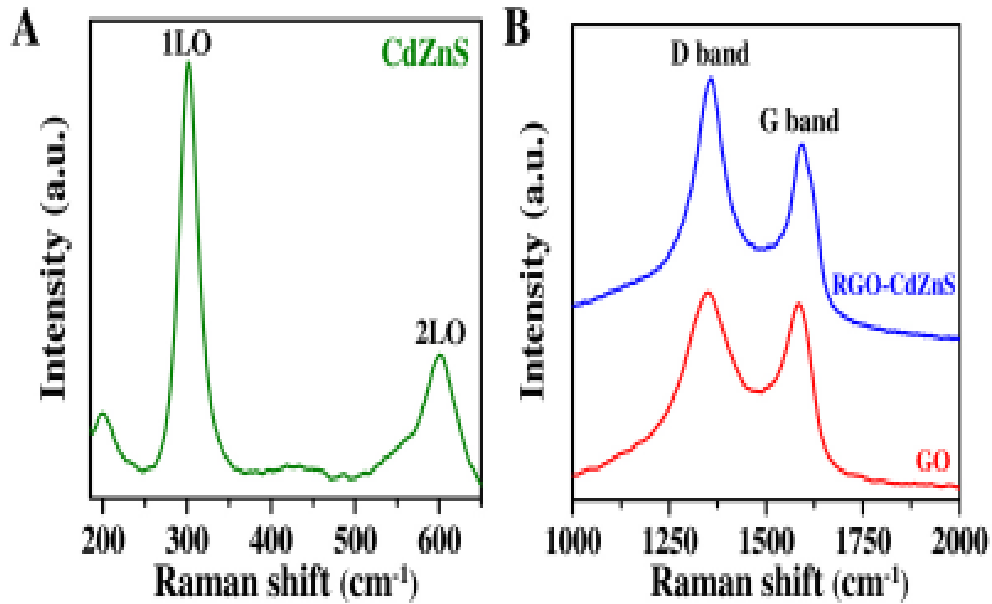


Figure 4.5.2: Micro-Raman spectrum of (A) $CdZnS$ (B) *GO* and *RGO* – $CdZnS$ composite.

The Raman spectra of *RGO – CdZnS* exhibited a significant increase of I_D/I_G (1.07) compared to *GO* (1.34), depicts the restoration of sp^2 domains upon reduction of *GO*.

The *UV – vis.* absorption spectra of controlled-*CdZnS* and *RGO – CdZnS* are compared in Figure 4.5.3A. The band-gap energy of controlled-*CdZnS* nanorod is calculated from the relation

$$(\alpha hv) = A(hv - E_g)^{1/2}$$

where α is the absorption coefficient; E_g is the band-gap of the material. Estimated value of E_g is nearly 3.1 eV, calculated from the $(\alpha hv)^2$ versus hv curve (inset of Figure 4.5.3A). As displayed in figure, it is obvious that after incorporating *RGO* in *CdZnS*, the absorbance increases in the region 280 – 600 nm compared to the controlled-*CdZnS*. The improvement of absorbance may be due to the synergistic effect of absorption contribution from *RGO* and *CdZnS*. Better absorbance ability is highly desirable to get efficient photo induced carrier generation. Thus it is expected that the synthesized *RGO – CdZnS* will be a potential candidate in the field of optoelectronics.

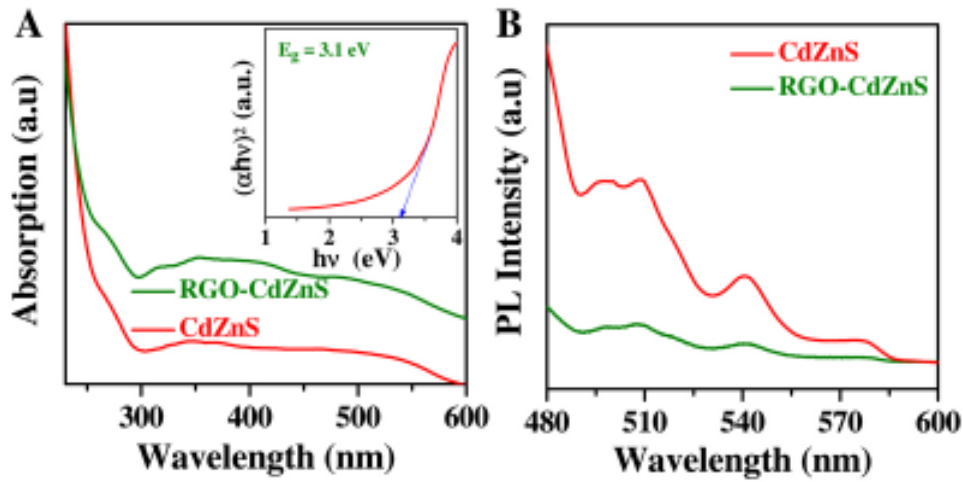


Figure 4.5.3: (A) Optical absorption spectra of controlled $CdZnS$ and $RGO - CdZnS$ composite. Plot of $(\alpha hv)^2$ vs photon energy (hv) for controlled- $CdZnS$ is shown in the inset of (A). (B) Photoluminescence spectra of controlled- $CdZnS$ and $RGO - CdZnS$ composite.

The significant electronic interaction among RGO and $CdZnS$ was confirmed by steady state PL study. Figure 4.5.3B compares the PL emission spectra of the controlled- $CdZnS$ and $RGO-CdZnS$. A very broad PL spectrum with four prominent peaks at 498, 509, 541 and 575 nm due to the surface defects are observed for controlled- $CdZnS$. The broad spectrum is may be due to wide range of size distribution of $CdZnS$ crystallites. Remarkably, the defect related emission becomes quenched for $RGO - CdZnS$, indicates the occurrence of photo induced charge or energy transfer among the interfaces [249]. The better photo induced charge transformation will give better photo current.

4.6 Photocurrent generation

The photoresponse of $RGO - CdZnS$ was studied on a thin film photodetector under simulated solar light. The cartoon of our photo detector along with electrical circuit is illustrated in Figure 4.6.1A. $I - V$ characteristics of $RGO - CdZnS$, measured both in dark and illuminated condition (Intensity: 80 to $160 mWcm^{-2}$) are shown in Figure 4.6.1B. All the curves are linear within the measurable voltage range ($\pm 2V$), demonstrating that the conduction is Ohmic both in darkness and illuminated condition. $I - V$ characteristic of controlled- $CdZnS$ thin film device, measured both in dark and illuminated condition ($100 mWcm^{-2}$) is shown in inset of Figure 4.6.1B.

The Photosensitivity (P), ratio of I_{Ph} and I_D , is one of the important figure of merit of a photo detector and here I_{Ph} is the photo current which can be obtained by the difference between current under illumination (I) and dark current (I_D) [$I_{Ph} = I_L - I_D$]. In our thin film we have noticed that P increases up to 47 % at the intensity of $160 mWcm^{-2}$.

A linear variation of P with the intensity of illuminated light is observed and which is presented in Figure 4.6.1C. The linear variation is advantageous for tuning the optoelectronics device performance [81]. The photocurrent generation mechanism in our composite system can be articulated with the help of band diagram and considering excitonic picture under illumination (inset of Figure 4.6.1C). After illumination of light, excitons (bound electron-hole pair) are formed at RGO and $CdZnS$.

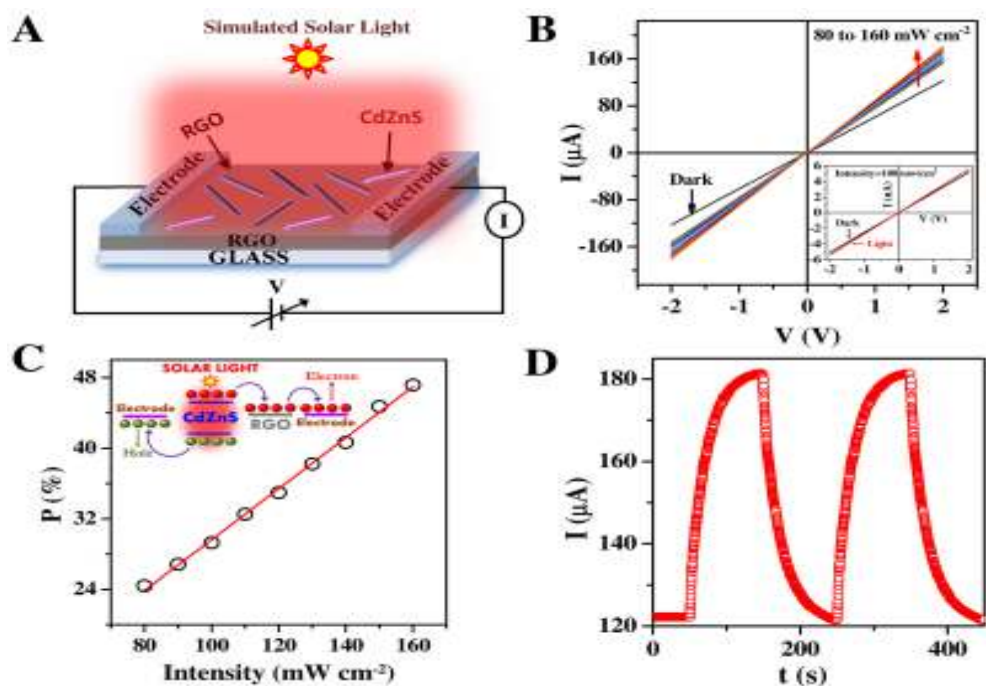


Figure 4.6.1: (A) The cartoon of our photo photodetector device along with the electrical transport measurement setup (B) $I - V$ characteristics for $RGO - CdZnS$ nanocomposite thin film device under dark condition and under different level of illumination intensity. $I - V$ characteristics for controlled- $CdZnS$ thin film device under dark and illumination condition is shown in the inset. (C) The variation of P with illuminated intensity of $RGO - CdZnS$ thin film device. Photocurrent generation mechanism in $RGO - CdZnS$ device is shown in inset C. (D) Current versus time for several cycles as the light was turned on and off.

The photo generated excitons are dissociated into free carriers at the interfaces and the defect states present in the thin film. The unique 2-dimensional structure of RGO initiates the favored interface with $CdZnS$ for excitons dissociation. For a pure semiconductor the electron-hole pairs have the tendency to recombine themselves, which decrease the possibility of photocurrent generation. In the RGO based composites, the free holes are collected at the negative electrode from the valence band of $CdZnS$,

while the electron can easily transfer from the conduction band of $CdZnS$ to the positive electrode through the RGO sheet and hinder the recombination probabilities. Figure 4.6.1D shows the dynamical photoresponse (bias voltage = $2V$) of $RGO - CdZnS$ thin film device under illumination intensity of $160 mW cm^{-2}$.

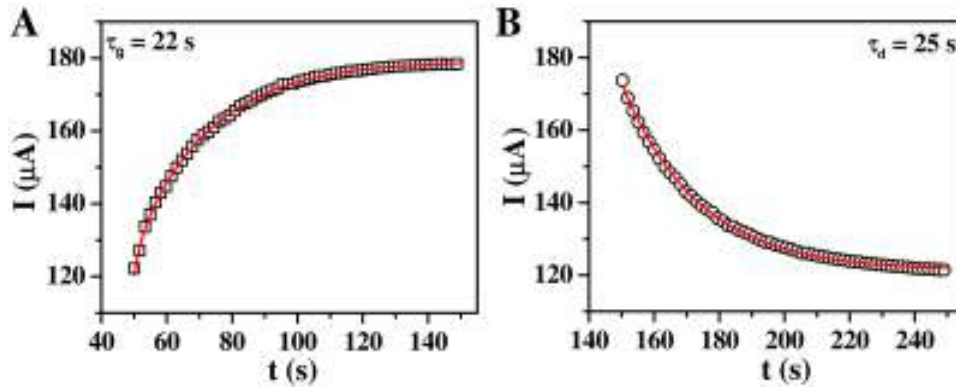


Figure 4.6.2: (A) Growth. (B) Decay of current in our $RGO - CdZnS$ thin film along with fittings of Eqn. 4.6.1 and 4.6.2 respectively.

The photodetector shows a stable and reproducible photoresponse upon repeated ON/OFF cycles of light with an interval of $100 sec$. As soon as the light source was turned ON the current increased and reached a steady value ($185 \mu A$). After turning OFF, it gradually reached the dark value ($122 \mu A$). Figure 4.6.2A and 4.6.2B depict the growth and decay current respectively. Dynamic photoresponse of $RGO - CdZnS$ under simulated solar light shows exponential behaviour and can be represented by the following relations

$$I(t) = I_{dark} + A \left\{ 1 - e^{\frac{-(t-t_0)}{\tau_g}} \right\} \quad (4.6.1)$$

$$I(t) = I_{dark} + B \left\{ e^{\frac{-(t-t_0)}{\tau_d}} \right\} \quad (4.6.2)$$

where, τ_g and τ_d time constants for growth and decay, A and B , the scaling constants, t_0 the time when the light was turned *ON* (growth) and *OFF* (decay). In Figure 4.6.2A and 4.6.2B, the solid lines are fit to the equation 4.6.1 and equation 4.6.2 respectively. The best fitted time constant of our device are obtained as $t_g = 22 \text{ s}$ and $t_d = 25 \text{ s}$.

4.7 Photocatalytic activity

The photocatalytic degradation of 4-*NP* at room temperature was studied in a glass photo reactor equipped with solar-light simulator, in the presence of *RGO* – *CdZnS* as photo catalyst. Samples were withdrawn at regular time intervals for the record of *UV-vis* absorption spectra by using a Shimadzu *UV* – 1700 spectrophotometer during the course of the irradiation (1 *h* overall). The quenching of absorption peak of 4-*NP* was monitored to study the photo degradation of 4-*NP*.

The photocatalytic degradation of 4-*NP* in presence of *NaBH*₄ is a model reaction to investigate the photocatalytic performance of a catalyst, which we have adapted here. The *UV* – *vis* absorption spectra of aqueous 4-*NP* solution shows an absorption peak located at 317 *nm*, which red shifted to 400 *nm* after the addition of *NaBH*₄ due to formation of 4-nitrophenolate ion and consequently the color of the solution changes from dull yellow to bright yellow. The peak position of the 4-nitrophenolate ion

remains unaffected after addition of *CdZnS* or *RGO – CdZnS* catalyst under dark condition. After shining simulated solar light, the 400 nm peak quenched gradually as the reaction time proceeds, indicates the occurrence of photo degradation of nitrophenol ion (Figure 4.7.1A and 4.7.1B). However, the absorption peak intensity remains unaffected for long time under similar reaction condition in absence of any catalyst. The degradation efficiency was calculated using the equation 2.4.4 [222, 238].

The degradation efficiency over illumination time of controlled-*CdZnS* and the *RGO – CdZnS* composite is compared in Figure 4.7.1C. It is observed that the degradation efficiency is only 63 % after 24 min of illumination for the controlled-*CdZnS* catalyst. Which enhanced upto 94 % for the *RGO – CdZnS* catalyst under similar experimental condition and same time span. The photo degradation kinetics is also expressed as the equation 2.4.5 [238, 250, 251]. The variation of $\ln(C_0/C)$ with time shows a linear behavior, which indicates the occurrence of pseudo-first order degradation kinetics of 4 – NP. The values of the degradation rate constants are calculated as $5 \times 10^{-2} \text{ min}^{-1}$ and $11 \times 10^{-2} \text{ min}^{-1}$ for controlled-*CdZnS* and *RGO – CdZnS* composite respectively.

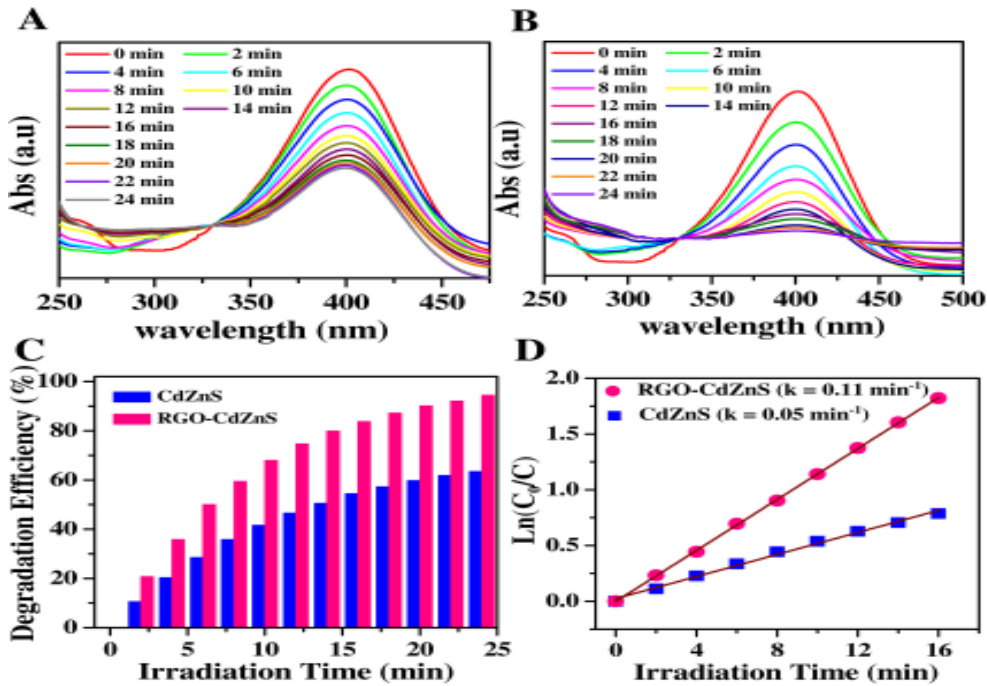


Figure 4.7.1: *UV – Vis* absorption spectra of 4-nitrophenol ion (A) controlled-*CdZnS* (B) *RGO – CdZnS* composite for different time of simulated solar light. The comparison of (C) the photo degradation efficiency and (D) $\ln(C_0/C)$ as a function of illumination time for the photocatalysis of 4 – *NP* solution containing *CdZnS* and *RGO – CdZnS* composite.

This enhancement of degradation rate constant for *RGO – CdZnS* composite is attributed to the synergetic effect of two factors, in one hand, the large surface area of *RGO* offers more photocatalytic reaction centers and subsequently enhanced photocatalytic activity. On the other hand, *RGO* serves as an acceptor of the photo induced electrons in *CdZnS* which hinders the recombination probability of the electron hole pairs. The recycling tests of *RGO – CdZnS* catalyst were performed to check the photo stability of the composite. Our result shows that recycled use of *RGO – CdZnS* for five times does not markedly affect its efficiency towards 4 – *NP* degradation.

4.8 Conclusion

In summary, solution processable $RGO-CdZnS$ nanorod composite material was successfully synthesized by single step one-pot solvothermal process. Formation of $RGO-CdZnS$ hybrid is confirmed by XRD . The Raman studies established the reduction of GO . TEM image confirms the attachment of $CdZnS$ nanorods onto RGO sheets. The TEM image analysis shows that $CdZnS$ nano rods of length $\sim 100\text{ nm}$ were anchored uniformly on the surface of RGO sheet, offering excellent support for interfacial contact. The photocatalytic activity of the $RGO-CdZnS$ nanocomposite has increased by 2.2 times in compared to controlled- $CdZnS$ samples towards the degradation of 4- NP . The recycle use of $RGO-CdZnS$ does not noticeably affect its photocatalytic efficiency. Our study has an enormous positive impact towards the removal of toxic water pollutant. The PL quenching and photoresponse study jointly corroborate the photo-induced charge generation and transfer along the interfacial contact. Large area thin film $RGO-CdZnS$ photodetector offers an enhanced photoresponse with P value is of 47 %, under 160 mWcm^{-2} light intensity. Dynamic photoresponse of $RGO-CdZnS$ under simulated solar light shows exponential behaviour and the time constants are 22 s and 25 s for growth and decay, respectively. Our study depicts that RGO play an important role toward enhancement of photocurrent generation in $RGO-CdZnS$ composite. Overall, the synergistic effect of RGO and $CdZnS$ in the composite is capable of getting promising applications in the field of optoelectronic devising.